DOE/SC-CM-18-003

U.S. DEPARTMENT OF ENERGY | Office of Science

FY 2018 Third Quarter Performance Metric: Demonstrate improved ocean circulation within Antarctic ice cavities when employing high-resolution configuration of E3SM-MPAS-Ocean

June 2018

Contents

Figures

Tables

1.0 Product Definition

Antarctica is surrounded by ice shelves that alter ocean properties and circulation through melting, freezing, and calving processes. These shelves extend over large ocean cavities, where warm waters melt the ice, in turn altering the shelf geometry and dynamics, with impacts on Antarctic-sourced sea-level rise (Asay-Davis et al., 2017). Ice shelves and ocean cavities in Antarctica have previously not been included in earth system models (ESMs) due to added model complexity and lack of observations for validation (Fyke et al., 2018). Ice shelves vary from 100 to 2000 m in thickness, and protrude over the ocean 30 to 600 km from the grounding line (the point where ice shelves come afloat). The two largest ice shelves, the Ross and Filchner-Ronne, are each the size of France. Waters from the Antarctic continental shelf flow into the ocean cavities below ice shelves, melting the ice and increasing in buoyancy because of the influx of freshwater (Figure 1a). The meltwater plume then ascends the ice-shelf base to the open ocean where it affects regional ocean properties. These sub-ice-shelf processes alter the temperature and salinity impacting ocean currents and mixing, which through the process of "water mass transformation" (Abernathey et al., 2016) eventually impact global ocean properties.

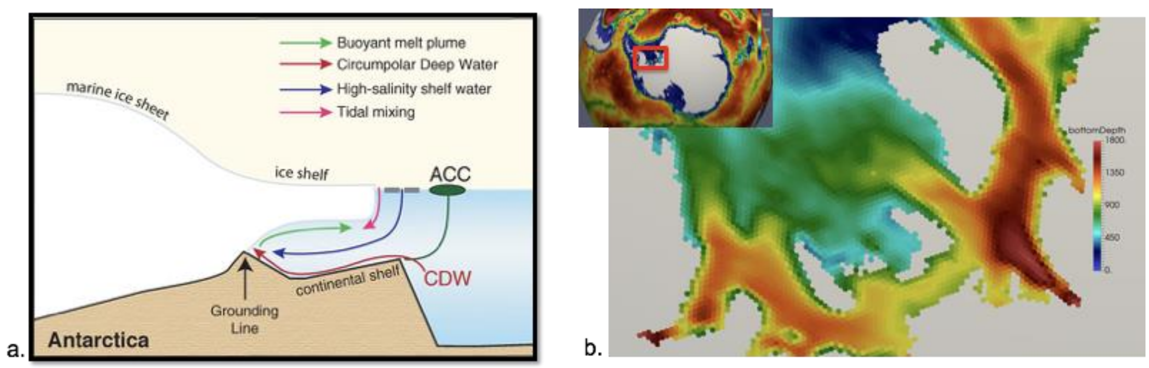

Figure 1. (a) Diagram of ocean circulation below an Antarctic ice shelf (Joughin et al., 2012). (b) Model bathymetry, fully below the Ronne-Filchner ice shelf, showing bedrock troughs (dark red/orange areas) near the grounding line (edge of grey cells) and individual 10 km-wide, hexagonal grid cells on the high-resolution unstructured horizontal mesh.

The U.S. Department of Energy's Energy Exascale Earth System Model (E3SM) can now be run in configurations that include ocean circulation within cavities below ice shelves so that these processes may be modeled explicitly, compared against observations, and then used in a predictive sense. This will lead to a better understanding of the potential for long-term changes in ocean circulation, ice shelf destabilization, and sea level rise. Here, we demonstrate that global simulations using high spatial resolution lead to improved representation of ocean properties proximal to and beneath ice shelves, leading to simulated sub-ice shelf melt rates that are also closer to observed values.

2.0 Product Documentation

This research improves upon standard IPCC-class simulations of the earth system by other groups, which do not include ocean cavities below ice shelves (Fyke et al., 2018). Rather, other models assume that the ocean domain ends as a vertical wall at the ice shelf edge, and the addition of basal melt water is simplistically included in the continental run-off parameterization at the ocean surface (Large and Yeager, 2009). Thus, standard models ignore the overturning circulation, the freshwater and salinity exchanges at depth beneath ice shelves, and the resulting feedbacks with regional ocean properties that follow from explicitly simulating melting and refreezing processes below the shelves.

The ocean component of E3SM, the Model for Prediction Across Scales (MPAS-Ocean, Ringler et al., 2013, Petersen et al., 2018), now has the capability to include ice shelf cavities within a global ocean domain and fully-coupled ESM simulations. The implementation relies heavily on the arbitrary Lagrangian-Eulerian vertical grid (Petersen et al 2015, Reckinger et al., 2015) and also required improvements for treating highly-tilted ocean layers, new methods for stable initialization of the ocean model under ice shelves, the addition of boundary layer physics for computing fluxes at the ice sheet and ocean interface, and the coupling of freshwater and salinity fluxes between the ice sheet and ocean at depth.

3.0 Detailed Results

Global E3SM simulations were conducted in two configurations: low resolution, where horizontal grid cell size varies from 60 km at mid-latitude to 30 km at high latitudes and below ice shelves (EC60to30); and high resolution, where grid cells scale with the Rossby radius of deformation from 30 km at the equator to 10 km at high latitudes and below ice shelves (RRS30to10). Simulations include active ocean and sea ice components (Petersen et al., 2018; Turner et al., 2018) with data (based on observed) atmospheric forcing and run-off from the Coordinated Ocean Research Experiments II (CORE-II) reanalysis (Large and Yeager, 2009). The ice shelf extent and depression are from observations (Fretwell et al., 2013) and remain static for the simulation. Basal melt rates are based on the model-simulated ocean temperature and salinity in the boundary layer at the base of the ice shelf (Holland and Jenkins, 1999).

The ocean was initialized with observed climatological temperature and salinity (Steele et al., 2001) and spun up for 15 years. The low- and high-resolution simulations were compared over years 15 to 30 for this analysis. Sea floor temperature on the Antarctic continental shelf is compared with observations from Schmidtko et al., 2014 (note that this data set does not include observations beneath the ice shelves, which are too sparse to determine a spatial pattern). Relatively warm CDW enters the continental shelf along the seafloor from the deep ocean, while waters exiting the shelves are expected to be colder and fresher (and hence more buoyant) due to basal melting. Figure 2 and Table 1 show that the high-resolution simulation compares better to observations than the low-resolution simulation, particularly in the Weddell Sea and east of the Antarctic Peninsula, where the low-resolution simulation is much too warm.

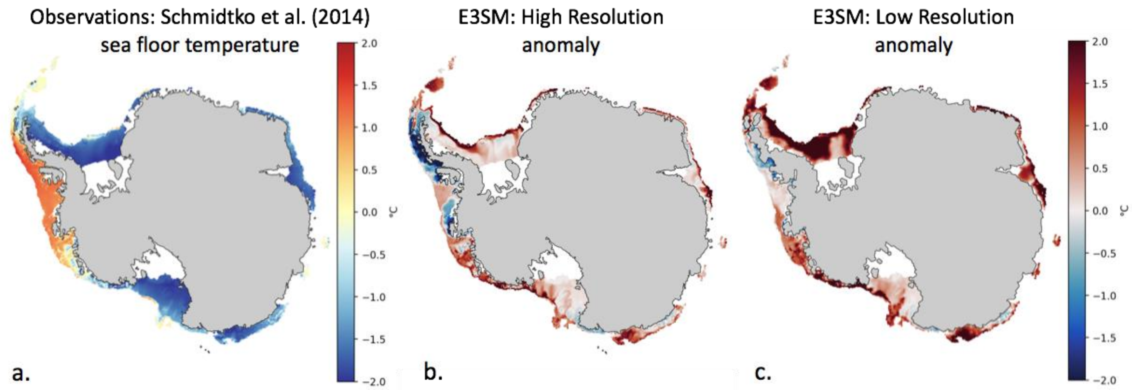

Figure 2. (a) Sea floor temperature from observations (Schmidtko et al., 2014). (b) The temperature anomaly (model minus observations) from E3SM high-resolution and (c) low-resolution simulations, averaged over 10 years. At high resolution, warm biases are smaller in magnitude and geographic distribution.

Table 1. Root-mean-square bias in seafloor temperature (°C), averaged over each region and over 20 simulated years. Bias is computed relative to observations (Schmidtko et al., 2014) as shown in Figure 2. Stepping from low to high resolution reduces the bias by 0.5-0.7 C.

Region:	Antarctica	West Antarctica	Peninsula	East Antarctica	Filchner-Ronne
Low Resolution	1.34	1.34	1.45	1.15	1.56
High Resolution	0.88	0.87	0.99	0.61	0.26

The Southern Ocean State Estimate (SOSE, Mazloff et al., 2010) uses an ocean model to assimilate available observations and provides the best available comparison and validation for the speed of ocean currents. The low-resolution E3SM mesh uses 30 km-wide grid cells in the Southern Ocean, which is larger than the Rossby radius of deformation, the length scale at which eddies may form. Thus the low-resolution simulation has low speeds and does not produce the turbulence and eddy structures visible in SOSE (Figure 3). Conversely, the high-resolution mesh, with 10 km cells, is able to reproduce the magnitude and overall pattern of the currents (Figure 3). Instantaneous images of the column-integrated speed show these turbulent structures throughout the Southern Ocean including currents that extend beneath the major ice shelves (Figure 4).

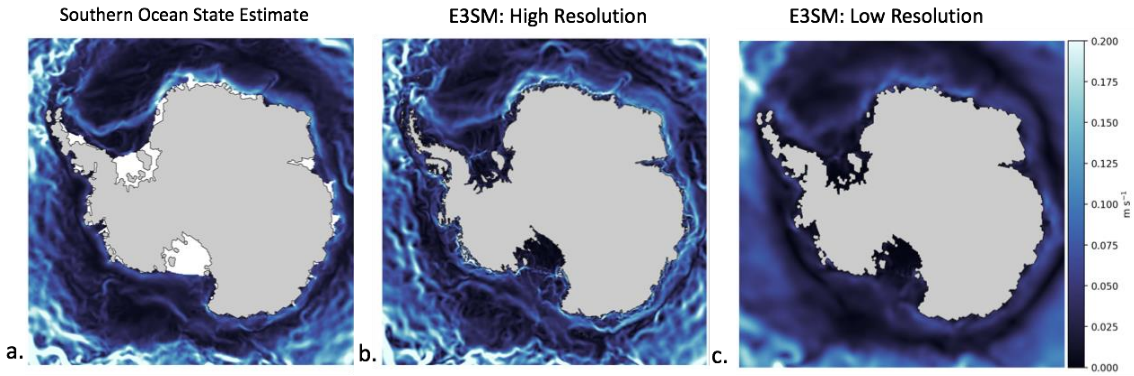

Figure 3. Sea surface velocity magnitude from the Southern Ocean State Estimate (Mazloff et al., 2010), based (a) on observations, (b) E3SM high resolution and (c) low resolution simulations, averaged over 10 years. High-resolution simulations produce eddy activity and currents (critical for mediating the flow of warm waters into ice-shelf cavities) at scales similar to SOSE, while these features are largely absent at low resolution.

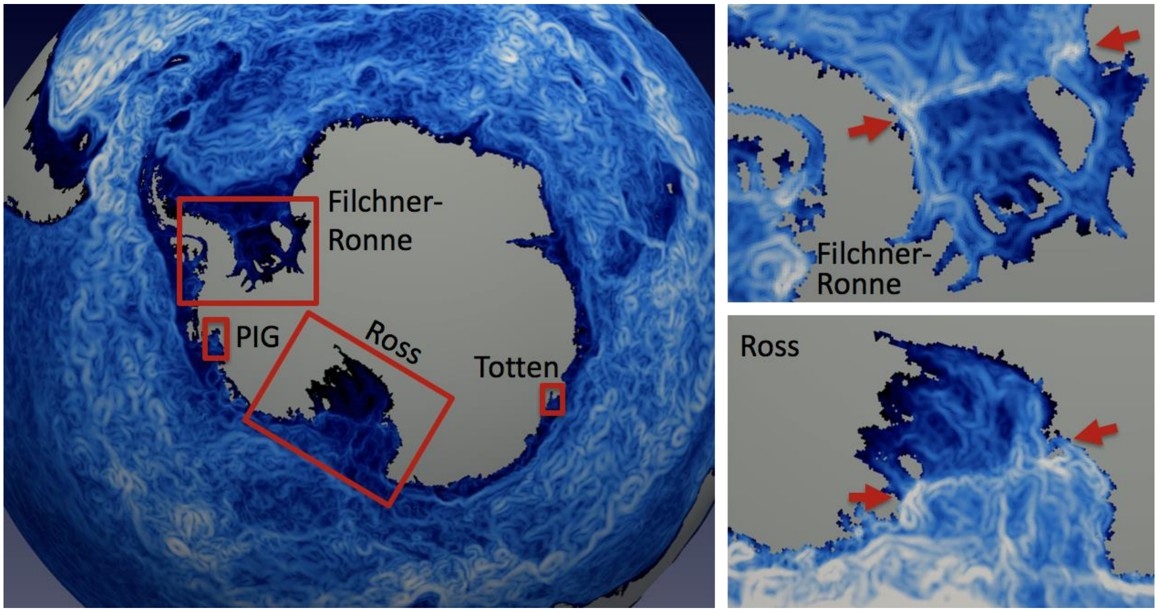

Figure 4. Instantaneous column-integrated ocean speed for the high-resolution simulation shows significant eddy activity throughout the Southern Ocean. Right panels reveal currents near and below the Filchner-Ronne and Ross ice shelves, where the shelf edge is denoted by arrows. White currents indicate column-integrated speeds of 500-2000 m^2/s on left panel and 30-100 m^2/s for right panels. Red boxes show locations of the two largest shelves, as well as for Pine Island Glacier (PIG) and Totten Glacier (for reference to Figure 5).

The average basal melt rate beneath ice shelves is an important overall metric for validation of these processes within a coupled model. It serves as an integrator of the relevant processes and their feedbacks and is also a primary term in the mass budget of the ice sheet (for Antarctica, ~½ of the freshwater flux to the oceans occurs through sub-ice shelf melt). Observational estimates from Rignot et al. (2013) were computed from surface accumulation, velocity, and satellite altimetry.

The low-resolution simulation melt rates are generally too low by a factor of 2-5, while the high-resolution melt rates are near to, or in some cases overlay the observations (Figure 5). Rignot et al. (2013) only provide the time-mean observed melt rate for each ice shelf, with estimated uncertainties. Conversely, simulated melt rates resolve both intra- and inter-annual variability, revealing the influence of warmer summer waters and longer timescale climate modes. More realistic melt rates in the high-resolution simulation are due to improved ocean properties of the currents entering the cavities, and smaller grid cells below the ice shelves so that the modeled melting may be resolved at finer spatial scales.

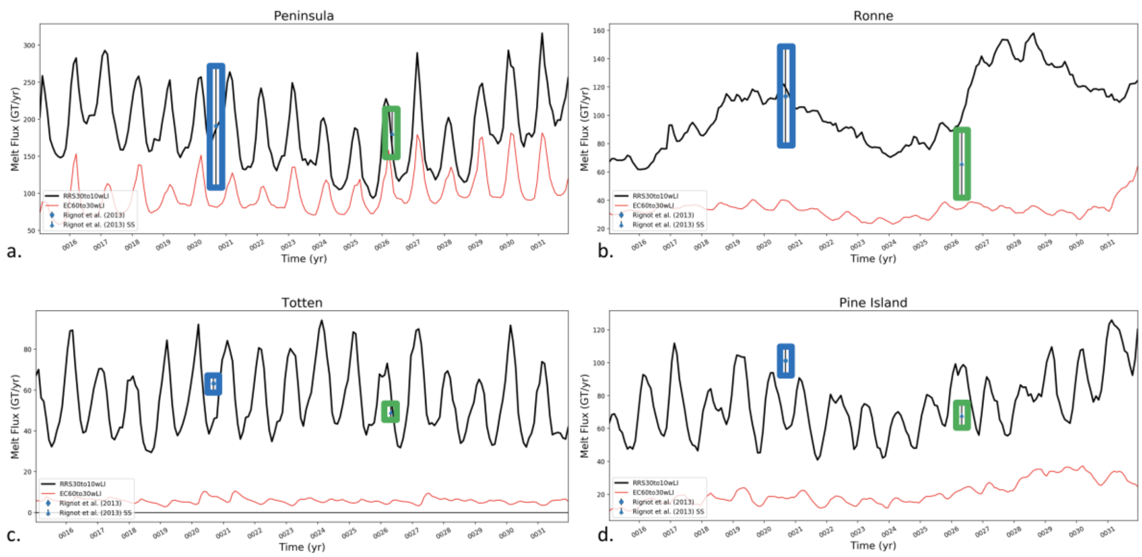

Figure 5. Melt rates averaged over specific ice shelves or regions of Antarctica. High-resolution (black) and low-resolution (red) simulations are shown for 15 years, for (a) the Antarctic Peninsula, (b) the Ronne, (c) Totten Glacier, and (d) Pine Island Glacier ice shelves. Time-averaged observations from Rignot et al. (2013) estimate non-steady state melt rates (i.e., observed, blue boxes) and steady-state melt rates (i.e., in the absence of observed ice shelf thinning, green boxes), where horizontal positions of boxes are arbitrary. In most locations, high-resolution simulations are closer to observations than the low-resolution results.

4.0 References

Abernathey, R. P., I. Cerovecki, P. R. Holland, E. Newsom, M. Mazloff, and L. D. Talley, 2016: Water-mass transformation by sea ice in the upper branch of the Southern Ocean overturning. *Nature Geoscience*, **9**, 596–601, doi:10.1038/ngeo2749.

Asay-Davis, X. S., N. C. Jourdain, and Y. Nakayama, 2017: Developments in Simulating and Parameterizing Interactions Between the Southern Ocean and the Antarctic Ice Sheet. *Curr. Clim. Change Rep.*, doi:10.1007/s40641-017-0071-0.

Fretwell, P., et al. (2013). “Bedmap2: improved ice bed, surface and thickness datasets for Antarctica”. *Cryosphere*, 7(1), 375-393

Fyke, J. G., O. Sergienko, M. Lofverstrom, S. F. Price, and J. Lenaerts, 2018: An overview of interactions and feedbacks between ice sheets and the Earth System. *Rev. of Geophys.* (in press).

Holland, David M., and Adrian Jenkins, 1999. Modeling Thermodynamic Ice–Ocean Interactions at the Base of an Ice Shelf. *Journal of Physical Oceanography* 29(8), 1787–1800. doi:10.1175/1520-0485(1999)029<1787:MTIOIA>2.0.CO;2.

Joughin, I., R. B. Alley, and D. M. Holland, 2012. Ice-Sheet Response to Oceanic Forcing. *Science* 338(6111), 1172–76. doi:10.1126/science.1226481.

Large, W., and S. Yeager, 2009: The global climatology of an interannually varying air–sea flux data set, *Climate Dyn*., 33(2-3), 341–364, doi:10.1007/s00382-008-0441-3.

Mazloff, M., P. Heimbach, and C. Wunsch, 2010: An eddy-permitting Southern Ocean state estimate, *J Physical Oceanography*, 40 (5), 880–899.

Orsi, A.H., Whitworth III, T., Nowlin Jr., W.D., 1995. On the meridional extent and fronts of the Antarctic Circumpolar Current. *Deep-Sea Research* I 42, 641–673.

Petersen, M.R., D.W. Jacobsen, T.D. Ringler, M.W. Hecht, M.E. Maltrud, 2015: Evaluation of the arbitrary Lagrangian–Eulerian vertical coordinate method in the MPAS-Ocean model. *Ocean Modelling*, **86**(0):93 – 113, doi:10.1016/j.ocemod.2014.12.004

Petersen, M., Asay-Davis, X., Berres, A., Comeau, D., Feige, N., Jacobsen, D., Jones, P., Maltrud, M., Ringler, T., Streletz, G., Turner, A., Van Roekel, L., Veneziani, M., Wolfe, J., Wolfram, P., Woodring, J. 2018: An evaluation of the ocean and sea ice climate of E3SM using MPAS and interannual CORE-II forcing. Submitting to *Journal of Advances in Modeling Earth Systems*. doi:10.5281/zenodo.1246339

Rignot, E., Jacobs, S., Mouginot, J., & Scheuchl, B. (2013). Ice-Shelf Melting Around Antarctica. *Science*, 341(6143), 266–270.

Ringler, T., Petersen, M., Higdon, R. L., Jacobsen, D., Jones, P. W., Maltrud, M., 2013: A multi-resolution approach to global ocean modeling. *Ocean Modelling*, **69**, 211–232.

Reckinger, S, Petersen, MR, Reckinger, SJ, A study of overflow simulations using MPAS-Ocean: Vertical grids, resolution, and viscosity, *Ocean Modelling*, **96**, Part 2, December 2015, 291-313

Schmidtko, S., Heywood, K. J., Thompson, A. F. & Aoki, S., 2014: Multidecadal warming of Antarctic waters. *Science* 346, 1227–1231.

Steele, M., R. Morley, and W. Ermold, 2001: PHC: A global ocean hydrography with a high-quality arctic ocean, *J. Climate*, 14(9), 2079–2087, doi:10.1175/1520-0442014<2079:PAGOHW>2.0.CO;2.

Turner, A.K., W.H. Lipscomb, E.C. Hunke, D.W. Jacobsen, N. Jeffrey, T.D. Ringler, J.D. Wolfe, 2018. MPAS-SeaIce: a new variable resolution sea-ice model. doi:10.5281/zenodo.1194374

U.S. DEPARTMENT OF
ENERGY

Office of Science